Topology of charge density and elastic properties of Ti_3SiC_2 polymorphs

R. Yu, X. F. Zhang
Materials Sciences Division, Lawrence Berkeley National Laboratory, Berkeley, CA94720

L. L. He, H. Q. Ye
Shenyang National Laboratory for Materials Science, Institute of Metal Research, Chinese Academy of Sciences, Shenyang 110016, China

(Date textdate; Received textdate; Revised textdate; Accepted textdate; Published textdate)

Using an all-electron, full potential first-principles method, we have investigated the topology of charge density and elastic properties of the two polymorphs, α and β, of Ti_3SiC_2. The bonding effect was analyzed based on Bader's quantum theory of "atoms in molecules" (AIM). It was found that the Ti-Si bonding effect is significantly weaker in β than in α, giving less stabilizing effect for β. The Si-C bonds, which are absent in α, are formed in β and provide additional stabilizing effect for β. In contrast to conventional thinking, there is no direction interaction between Ti atoms in both α and β. The calculated elastic properties are in good agreement with the experimental results, giving the bulk modulus of about 180 GPa and the Poisson's ratio of 0.2. The β phase is generally softer than the α phase. As revealed by the direction dependent Young's modulus, there is only slight elastic anisotropy in Ti_3SiC_2. For α, Young's modulus is minimum in the c direction and maximum in the directions 42° from c. For β, the maximum lies in the c direction, in part due to the formation of Si-C bonds in this direction.

Keywords: topology of charge density; electronic structure; elastic constants; ceramics.

I. INTRODUCTION

The layered ternary carbides and nitrides, e.g. Ti_3SiC_2, Ti_2AlC, Ti_3AlC_2, and Ti_4AlN_3 etc., have been the subject of numerous studies in recent years due to their unique combination of mechanical, electrical and thermal properties.[1–9] Among the compounds, Ti_3SiC_2 has the best comprehensive properties and thus has been investigated most extensively. It has high elastic moduli and easy machinability, good thermal and electrical conductivities, together with excellent oxidation properties and fatigue resistance.[1] In fact, Ti_3SiC_2 has become the model material of the layered ternary compounds.

There are two polymorphs[10–12] for Ti_3SiC_2, α and β phases. The structures for both α and β polymorphs are hexagonal in symmetry with a space group of $P6_3/mmc$ (No. 194). However, Si occupies 2b Wyckoff position in α, but 2d in β. Note that the 2b and 2d sites are the largest holes in α and β, respectively. The fact facilitates the transition between the two polymorphs. The unit cells of the two polymorphs are schematicaly shown in Fig. 1 (a) and (b). They can be described as an alternative stacking of the Ti and Si layers: AB<u>A</u>BAC<u>A</u>C for α and AB<u>C</u>BAC<u>B</u>C for β. The underlined letters refer to the layers of Si atoms; the remainders being the layers of Ti atoms. Carbon atoms occupy the octahedral interstitial sites of Ti atoms and are not shown in this notation.

The possibility of the presence of the β polymorph was first proposed by Farber et al.[10] In the early high-resolution transmission electron microscopy (HRTEM) investigations of Ti_3SiC_2, there was misinterpretation for the HRTEM images: the α polymorph was thought as the β polymorph[10]. Using image simulations, Yu et al.[11–12] clarified the relationship between HRTEM images and the underlying crystal structure for Ti_3SiC_2, and pointed out that the bright spots in HRTEM images do not necessarily correspond to the atomic columns. In the same work, they identified the existence of the β polymorph. Because β is less frequently observed[11] than α, it was proposed to be a metastable phase, which was confirmed by the first-principles calculations of the heats of formation[12] and the Gibbs free energy.[13]

Due to the improvements in theory, calculation methods, and computer size and speed, first-principles calculations are becoming a powerful tool for understanding and predicting structures and properties of materials.[14] Calculation results on Ti_3SiC_2 have been reported in literatures,[8,9,12,13,15,16] but mainly for the α phase. In the present work, we calculated the topology of charge density based on Bader's quantum theory of "atoms in molecules" (AIM)[17–19] and the elastic properties of the polymorphs. The chemical bonding and the electronic structure are analyzed comparatively in detail.

II. CALCULATIONS

A. Computational details

The full-potential linearized augmented plane waves (FLAPW) method[20–22] was used in this study. This method is one of the most accurate schemes to solve the Kohn-Sham equations in density-functional theory.[23–24] Augmented plane wave plus local orbitals (APW+lo) were used for valence states; LAPW were used for the other states. The use of the mixed LAPW/APW+lo basis set requires considerably less basis functions compared to the pure LAPW basis set.[25–26] In the present study, about 75 basis functions per atom were used. The gen-

eralized gradient approximation (GGA) exchange correlation functional of Perdew, Burke and Ernzerhof was used.[27] A fully relativistic calculation was used for core states, whereas the valence states were treated in a scalar relativistic scheme. The total and partial densities of states (DOS) were obtained using a modified tetrahedron method of Blöchl *et al.*[28] Tests on the k-point sampling in the Brillouin zone were performed to ensure that the total energies were converged to 0.1 mRy/atom.

B. Structural optimization and heats of formation

The structural optimization for Ti_3SiC_2 started with the structure parameters determined using X-ray diffraction.[29] The whole relaxation process includes four steps: (1) The atomic coordinations were relaxed with fixed lattice parameters; (2) With the fixed experimental c/a ratio and the atomic coordinations obtained in the previous step, the theoretical volume was obtained from volume-total energy curve; (3) Using the obtained theoretical volume and atomic coordinations, the total energy was calculated as a function of c/a ratio; (4) The atomic coordinations were relaxed again with the fixed theoretical lattice parameters.

The heats of formation were obtained by subtracting the total energies of the elemental crystals from the total energies of Ti_3SiC_2 polymorphs. In order to precise the total energies, all the elemental crystals were also fully relaxed. For titanium and graphite, the relaxation process was similar to that for Ti_3SiC_2, but simpler because there are no free internal coordinations for titanium and graphite.

C. Topology of electron density

In addition to band structure and density of states (DOS), electronic structure and chemical bonding of Ti_3SiC_2 were investigated quantitatively on the basis of Bader's quantum theory of "atoms in molecules" (AIM),[17−19] which is a theory about atoms, bonds, structure, and structural stability. Based on the topology of electron density, which can be obtained from either quantum mechanics computations or accurate experiments, the theory provides vigorous definitions for atoms in molecules/crystals and the bonds which link the atoms, and thus transform the qualitative concepts into a quantitative description. As its name, the AIM theory concerns mainly molecular quantum chemistry. Recently, the theory was also applied to solid-state phases.[30−35]

An atom in a molecule or crystal is an open system, which is free to exchange charge and momentum with neighboring atoms. In the AIM theory, an atom is defined as a region containing a single nucleus, with the flux in the gradient vector field of the electron density $\rho(\mathbf{r})$ vanishing at its surface, i.e.

$$\nabla\rho(\mathbf{r}) \cdot \mathbf{n}(\mathbf{r}) = 0 \tag{1}$$

where $\mathbf{n}(\mathbf{r})$ is the exterior normal vector to the surface of the region.

Once the atomic basins are determined an atomic properties of each atom can be obtained by integration of a corresponding property densities over the basin of the atom, and each atom makes an additive contribution to the value of the property of the total system. The electron population in atom Ω, for example, is given as

$$N(\Omega) = \int_{\Omega} \rho(\mathbf{r}) d\mathbf{r} \tag{2}$$

In addition to the definition of atomic basins, the topology of electron density gives the definition of molecular structure in terms of its critical points, where the gradient of the electron density vanishes, i.e.

$$\nabla\rho(\mathbf{r}) = 0 \tag{3}$$

According to Bader's notation, the critical points are characterized by the rank and signature of the Hessian matrix ($\nabla\nabla\rho(\mathbf{r})$) of the electron density. The rank is the number of non-zero eigenvalues of $\rho(\mathbf{r})$ and the signature is the number of positive eigenvalues minus the number of negative ones. In general, the critical points of electron density for energetically stable molecules or crystals are all of rank three, and there are just four possible signature values, i.e. four kinds of critical points: (3,-3) or local (nucleus or non-nucleus) maxima, (3,-1) or bond critical points (BCP), (3,1) or ring critical points (RCP), and (3,3) or cage critical points(CCP). The eigenvalues are generally denoted as λ_i (i=1-3) in an increasing order. Thus for a BCP, $\lambda_1 \leq \lambda_2 < 0 < \lambda_3$. For molecules or crystals with equilibrium geometry, the existence of a BCP indicates the formation of a bond between two neighboring atoms.

D. Elastic constants and Debye temperature

We calculated the single crystal elastic constants in terms of the linear theory of elasticity. For a small lattice distortion near equilibrium structure, the strain energy is[36−37]

$$E_{total} = \frac{1}{2} V \sum_{i,j} c_{ij} \epsilon_i \epsilon_j \tag{4}$$

where V denotes the volume of undistorted system, c_{ij} the elastic stiffness constants, and ϵ_i and ϵ_j the components of the strain tensor in the matrix form

$$\mathbf{e} = \begin{pmatrix} \epsilon_1 & \frac{1}{2}\epsilon_6 & \frac{1}{2}\epsilon_5 \\ \frac{1}{2}\epsilon_6 & \epsilon_2 & \frac{1}{2}\epsilon_4 \\ \frac{1}{2}\epsilon_5 & \frac{1}{2}\epsilon_4 & \epsilon_3 \end{pmatrix} \quad (5)$$

We use the method described in section A to calculate E_{total} for various strains of the system and find the second derivatives of the energy with respect to the strain. Then the elastic constants c_{ij} are evaluated using the equation (4). To find the distorted lattice vectors we adopt the matrix procedure given by Jona and Marcus,[38] who modified the procedure of Fast et al.[39] to get higher symmetry in distorted structures. In summary, the undistorted structure is written in a matrix form as

$$R = \begin{pmatrix} a\cos 15^\circ & a\sin 15^\circ & 0 \\ a\cos 75^\circ & a\sin 75^\circ & 0 \\ 0 & 0 & c \end{pmatrix} \quad (6)$$

where a and c are lattice constants.

The distorted structure R' is then ontained by

$$R' = R(I + \mathbf{e}) \quad (7)$$

where I denotes the unit matrix. Since there are five independent elastic constants for the hexagonal phase, five different strains are needed. The five strains and the related elastic constants (in parentheses) are listed as follows:

(i) $\epsilon_1 = \epsilon_2 = \epsilon$, $(c_{11} + c_{12})$
(ii) $\epsilon_3 = \epsilon$, (c_{33})
(iii) $\epsilon_1 = \epsilon_2 = \epsilon_3 = \epsilon$, $(2d_{11} + 2d_{12} + 4c_{13} + c_{33})$
(iv) $\epsilon_4 = \epsilon_5 = \epsilon$, (c_{44})
(v) $\epsilon_1 = -\epsilon_2 = \epsilon$, $(c_{11} - c_{12})$

In each above case, the other components of the strain tensor are equal to zero. Different strain from that of Jona and Marcus[38] is used to calculate $c_{11} - c_{12}$. Using the present strain, the energy of the distorted structure becomes an even function of the strain. Therefore, only strains in one direction are needed. All the distorted structures were relaxed with respect to internal coordinates to obtain accurate elastic constants.

Polycrystalline elastic constants can be evaluated on the basis of single crystal elastic constants. In this study, the bulk modulus (B) is calculated directly from case (iii) strains ($9B = 2d_{11} + 2d_{12} + 4c_{13} + c_{33}$), the shear modulus ($G$) is obtained by averaging schemes developed by Voigt (G_V),[40] Reuss (G_R),[41] and Hill.[42] In Voigt approximation, the shear modulus (G_V) of polycrystals is assumed to be the space average of stiffness c_{44} of crystallites disposed at all possible orientations. The Voigt approximation is equivalent to assuming that the strain is uniform throughout the aggregate, but the stress is not. On the other hand, assuming uniform stress but non-uniform strain, the shear modulus (G_R) is taken as the reciprocal space average of compliance s_{44} of the crystallites. For hexagonal crystals:

$$G_V = [(2d_{11} + c_{33}) - (c_{12} + 2d_{13}) + 3(2d_{44} + c_{66})]/15 \quad (8)$$

$$1/G_R = [4(2s_{11} + s_{33}) - 4(s_{12} + 2s_{13}) + 3(2s_{44} + s_{66})]/15 \quad (9)$$

where s_{ij} are elastic compliances. Using an energy argument, Hill[42] proved that G_V and G_R represent upper and lower limits and the true value of G should lie between them. Emperically, a good approximation is

$$G = (G_V + G_R)/2 \quad (10)$$

Young's modulus (E) and Poisson's ratio (ν) are given by:

$$E = \frac{9BG}{3B + G} \quad \text{and} \quad \nu = \frac{3B - 2G}{2(3B + G)} \quad (11)$$

The Debye temperature (θ_D), a fundamental parameter of a solid, can also be calculated from elastic constants employing the relationship between θ_D and the sound velocity.[43] The polycrystalline shear, υ_s, and longitudinal, υ_l, sound velocities are computed from B and G as follows:

$$\upsilon_s = (G/\rho)^{1/2} \quad (12)$$

$$\upsilon_l = ((B + 4G/3)/\rho)^{1/2} \quad (13)$$

The mean sound velocity υ_m is

$$\upsilon_m = \left(\frac{1}{3}\left[\frac{2}{\upsilon_s^3} + \frac{1}{\upsilon_l^3}\right]\right)^{-1/3} \quad (14)$$

Then the Debye temperature is given by the equation:

$$\theta_D = \frac{h}{k}\left(\frac{3qN\rho}{4\pi M}\right)^{1/3} \upsilon_m \quad (15)$$

where h denotes Planck's constant, k Boltzmann's constant, N Avogadro's number, ρ the density, M the molecular weight of the solid and q the number of atoms in the molecule.

III. RESULTS AND DISCUSSIONS

A. Structural optimization and heats of formation

The calculated and the experimental lattice parameters and atomic positions of Ti_3SiC_2 are listed in Table I. Note that the calculated C positions are very close to

those determined recently by neutron diffraction,[44] but are significantly different from those determined earlier by X-ray diffraction.[26] In contrast to the fact that the X-ray scattering factor of C is much smaller than those of Ti and Si, the neutron scattering factors of the three elements are similar.[45] Therefore, the positional parameters of the light carbon atoms determined from neutron diffraction are generally more precise than those determined from X-ray diffraction, especially for powder diffraction. The agreement between the calculated C positions and those determined by neutron diffraction demonstrates the accuracy of the geometrical relaxation of the first-principles calculations.

Table II gives the total energies of Ti_3SiC_2 and elemental crystals, from which the heats of formation of Ti_3SiC_2 are obtained as listed in Table II. The heat of formation for the α phase is -81.2 kJ/mol, while that for β is -75.7 kJ/mol, confirming the metastability of the β phase.[11−12]

B. Charge density and it's topology

The calculated valence charge densities in $(11\bar{2}0)$ plane of the polymorphs are given in Figs. 2(a) and 2(b). In order to visualize the reordering of the electronic charge density accompanying the formation of bonding, the difference charge densities were obtained by subtracting the superposition of free atom densities from the total valence charge density. The results are shown in Figs. 3(a) and 3(b). The electron density maps show some common features of the two polymorphs. For example, as demonstrated by the difference charge densities, there exists a significant charge transfer from Ti to C; The Ti-C-Ti bonding demonstrates large directionality, a character of covalent bonding.

In Fig. 3(b), the charge accumulation between Si and it's next-nearest-neighboring C atoms can be observed in the β phase. Such accumulation suggests the formation of Si-C bonding in β, which is confirmed in the following topology analysis (AIM).

The crystallographically inequivalent BCPs, denoted by the atoms they connect, are listed in Table III. The bond length, electron density, eigenvalues of Hession of ρ, laplacian (sum of eigenvalues) and the ratio $|\lambda_1|/\lambda_3$ are given.

First we notice that a new BCP connecting Si and C atoms exists in β, indicating the formation of Si-C bonds, which are absent in α. The Si-C bonding could provide additional stabilizing effect for β. But from the heats of formation we know that the β phase is a metastable phase relative to α. By examining the properties of the BCPs, it is found that the electron density at the Ti2-Si BCP in β is significantly smaller than in α. It means that less charge is accumulated in the bonding region between Ti2 and Si atoms in β, giving weaker and longer Ti2-Si bond, and weak stabilizing effect for β.

Since the Si-C bonds exist only in the β phase, the transformation from one polymorph to the other should involve bond breaking and rearrangement. That means the transformation is reconstructive, although the two polymorphs differ slightly in structure. Furthermore, such a reconstruction can not be accomplished by a homogeneous distortion, like in Martensitic transformations.[46] Instead, the diffusion of Si atoms is required, Si atoms hop from normal 2b sites to 2d sites (the largest holes in α) to generate Frenkel defects (vacancies at 2b and interstitials at 2d). A Frenkel defect in α can be regarded as a β nucleus of a half unit cell.

From the bond lengths of Ti_3SiC_2 listed in Table III, it is noticed that Ti1-C bond is longer and has a smaller electron density relative to Ti2-C bond in both α and β. This might be attributed to the weaker Ti2-Si bonding relative to Ti2-C bonding, resulting in a charge transfer from the former to the latter. Thus the Ti2-C bonding is strengthened.

According to the topology properties at BCPs, there are two categories of interatomic interactions: shared interaction and close-shell interaction.[17] For a BCP of shared interaction, the laplacian is negative, the election density is large (order 1 in $e\text{Å}^{-3}$), and the ratio $|\lambda_1|/\lambda_3$ is larger than unity, corresponding to covalent bonds. Close-shell interaction means positive laplacian, lower electron density and a smaller ratio $|\lambda_1|/\lambda_3$ at the BCPs. Ionic bonds, hydrogen and Van der Waals bonds fall in this category. According to these definitions, all the bonding interactions in Ti_3SiC_2 belong to close-shell interaction. This is in accordance with the large charge transfer between the atoms of Ti_3SiC_2, as listed in Table IV.

The above classification scheme, like other bonding classification schemes, is not a quantitatively rigorous scheme, but a qualitative one for easy understanding. Not all the bonds can be classified unambiguously in such a way. For example, due to the strong covalent interaction between Ti and C, the charge densities at Ti1-C and Ti2-C BCPs are not small enough as for typical ionic bonds.

Si-Si and Si-C bonds are typical covalent bonds in Si and SiC crystals. However, they are categorized as close-shell interaction in Ti_3SiC_2. Although this should not be regarded as the failure of above classification scheme since both the Si-C and Si-Si bond lengths here are much larger than their normal values (2.35 Å in Si and 1.89 Å in SiC), it suggests the necessity to generalize above scheme developed from molecular quantum chemistry by taking into account the constraints the atoms receive in crystals.

Finally, it should be noted that there is no direct Ti-Ti bonding interactions in Ti_3SiC_2. While it's in contrast to traditional thinking, we will show that it's a common feature in most of the transition metal carbides and nitrides.[47]

TABLE I: Experimental and calculated lattice parameters (a, c in nm), atomic positions (in fractional coordination) of Ti_3SiC_2. For both α and β, Ti1 and Ti2 refer to the Ti atoms occupy 2a Wyckoff position (0, 0, 0) and 4f position (1/3, 2/3, z), respectively. C atoms also occupy 4f position, but with different z value from that of Ti2. Si atoms occupy 2b position (0, 0, 1/4) in α, while 2d position (2/3, 1/3, 1/4) in β.

		a	c	c/a	z_{Ti2}	z_C
α	Neutron diffraction[44]	0.307	1.763	5.75	0.135	0.572
	X-ray diffraction[25]	0.307	1.767	5.76	0.135	0.568
	Calculation	0.308	1.772	5.75	0.135	0.573
β	Calculation	0.306	1.807	5.91	0.134	0.571

TABLE II: Calculated lattice parameters (a, c in nm), total energies (E in Ry), and heats of formation (ΔH in kJ/mol) of Ti_3SiC_2 and the elemental crystals.

	a	c	E	ΔH
α	0.308	1.772	-11711.428	-81.2
β	0.306	1.807	-11711.376	-75.7
Ti	0.243	0.466	-3415.244	
Si	0.547		-1160.140	
C	0.247	0.672	-304.815	

C. Band structure and DOS

The band structures of α and β are shown in Figs. 4(a) and 4(b), respectively. The four lower and the next two bands are s states of C and Si atoms. The dispersion of Si s bands is larger than that of C s bands due to the more diffuse character of the Si s orbitals. The higher bands from about -6.0 eV are valence Ti $3d$ and (Si, C) p states. Due to the large dispersion of Si s states, no energy gap is formed between the lower s bands and the higher p and d bands.

By comparing the band structures of the two polymorphs, the differences in orbital interactions are revealed. It is found that, at K and H points, the bands near -2.1 eV in α increase to near -1.4 eV in β, while those close to the Fermi level of α decrease to -0.3 eV in β. From the band character plotting, as shown in Figs. 5(a)-5(d) for β, the compositions of the featurered bands are obtained. The figures show that the bands of β near -1.4 eV consist mainly of the contributions from the states C $2p_z$, Si $3p_z$, and Ti2 $3d_{xz}$+$3d_{yz}$, which form the interactions between base planes. The bands near -0.3 eV consist mainly of the contributions from $3d_{xz}$+$3d_{yz}$ and $3d_{x^2-y^2}$+$3d_{xy}$ of Ti2 atoms, which interact within the base planes. Because of the decreased electron density between Si and Ti2 atoms in β (Fig. 2(b) and Fig. 3(b)), the interplane bonding interactions between Si $3p_z$ and Ti2 $3d_{xz}$+$3d_{yz}$ are weak in the β phase. The energy of these interactions increase from -2.1 eV in α to -1.4 ev in β. The Si-C interactions in β are not strong enough to stabilize the interplane interactions. The energy of the bands near Fermi level of α decreases by about -0.3 eV, demonstrating that the interactions within the base planes are stabilized.

Many features in band structures can also be illustrated in electron densities of states (DOS), as shown in Fig. 6(a) and 6(b). Corresponding to the shift of Si $3p_z$ band near K and H points, the highest peak of Si $3p$ shifts from -2.1 eV in α to -1.4 eV in β. The minor peak of Ti2 atoms also shifts due to the Si-Ti2 hybridization. Similarly, corresponding to the shift of $3d_{xz}$+$3d_{yz}$ and $3d_{x^2-y^2}$+$3d_{xy}$ bands of Ti2 atoms, the peak near the Fermi level of α shifts down to -0.3 eV in β, resulting in a decrease of $N(E_F)$, the DOS at the Fermi level, from 4.4 states/(unit cell eV) for α to 3.6 for β. The lower $N(E_F)$ may lead to lower conductivity of β relative to α.

The partial DOS (PDOS) curves do not show detectable hybridization between Si s states and the electronic states of Ti and C atoms. It means that the dispersion of Si s bands originates mainly from the two-dimensional interaction within the Si planes. Due to Bloch's theorem, a phase factor is associated to every translation.[48–49] At K point ($2\pi/3$, $2\pi/3$, 0) in the Brillouin zone of Ti_3SiC_2, the phase factor linking a Si s orbital with its neighbor is equal to $e^{\pm i2\pi/3}$ and so the Bloch function looks like that shown in Fig. 7, where the phase is denoted by different colors. Therefore, the interactions between all the nearest neighbouring s orbitals are antibonding, and the K point should be at the top of Si s band as shown in Fig. 4.

D. Elastic properties

Because of the difficulty to grow Ti_3SiC_2 single crystals, there are only polycrystalline elastic constants available from the reported experiments.[50–53] However, single crystal elastic constants can be obtained from first principle calculations. The elastic constants of Ti_3SiC_2 were calculated using the pseudopotential method[7,13]. In the present study, we adopted the all-electron F(L)APW+lo method[21] to calculate the single crystal elastic constants. The results are given in Table V. Polycrystalline elastic constants, sound velocities and Debye temperature were calculated from the single crystal elastic constants as listed in Table VI. The calculated values match the experimental data very well. For example, the bulk modulus of the α phase was measured experimentally,[50–52] most of the results, including the latest one,[53] showed a

TABLE III: Bond length (l in Å), electron density (ρ in eÅ^{-3}), eigenvalues of Hessian and laplacian (λ_i, $\nabla^2\rho$ in eÅ^{-5}) of ρ, and the ratio $|\lambda_1|/\lambda_3$ at the bond critical points in Ti_3SiC_2 polymorphs.

	Bond	l	ρ	λ_1	λ_2	λ_3	$\nabla^2\rho$	$\lvert\lambda_1\rvert/\lambda_3$
α	Ti1-C	2.20	0.473	-1.62	-1.57	5.42	2.23	0.30
	Ti2-C	2.10	0.576	-2.06	-2.06	5.56	1.44	0.37
	Ti2-Si	2.70	0.269	-0.64	-0.53	2.18	1.00	0.29
	Si-Si	3.08	0.198	-0.21	-0.12	0.78	0.45	0.27
β	Ti1-C	2.18	0.483	-1.67	-1.62	5.49	2.20	0.30
	Ti2-C	2.10	0.589	-2.22	-2.14	5.48	1.12	0.41
	Ti2-Si	2.75	0.239	-0.42	-0.40	2.03	1.22	0.21
	Si-Si	3.06	0.194	-0.22	-0.10	0.81	0.49	0.27
	Si-C	3.23	0.206	-0.19	-0.19	1.05	0.67	0.18

TABLE IV: Atomic charges for Ti_3SiC_2 polymorphs.

	Ti1	Ti2	Si	C
α	1.623	1.421	-0.874	-1.795
β	1.633	1.363	-0.800	-1.779

B value of close to 180 GPa, matching well with present calculations. Comparison between the two polymorphs shows that the β phase is generally a little softer than the α phase.

The Cauchy relations were examined. For hexagonal materials it was demonstrated that the following Cauchy relations held if the interatomic forces were central: $c_{12} = c_{66} = (c_{11} - c_{12})/2$ and $c_{13} = c_{44}$, *i.e.*, the Cauchy ratio (c_{12}/c_{66} and c_{13}/c_{44}) was unity. The Cauchy ratio shown in Table V indicates that its deviation from unity is notable, similar to many hexagonal transition metals.[39]

Elastic anisotropy exists in real crystals and plays an important role in determining properties of crystals. Here we calculate the change of Young's modulus with direction to investigate the elastic anisotropy in Ti_3SiC_2. For hexagonal systems, the reciprocal of Young's modulus (E) in the arbitrary direction is defined as[36]

$$1/E = (1 - l_3^2)^2 s_{11} + l_3^4 s_{33} + l_3^2(1 - l_3^2)(2s_{13} + s_{44}) \quad (16)$$

Note that the Young's modulus of hexagonal crystals depends only on one direction cosine, $l_3 = \cos\theta$, where θ is the angle between the arbitrary direction and the crystallographic c-axis. This is because the hexagonal crystals are isotropic in the basal plane. The direction dependent Young's modulus of Ti_3SiC_2 is shown in Figs. 8(a) and 8(b) for α and β, respectively. From these figures one can see that the Young's modulus of the α phase is larger in directions between the a and c axis, the minimum of 303 GPa is in the c direction, and the maximum of 355 GPa in the directions 42° from c. In contrast, the Young's modulus of the β phase is smaller in directions between the a and c axes, maximum (325 GPa) in c and minimum (300 GPa) in the directions 50° from c. It's interesting to note that, although the β phase is generally softer than the α phase, it's Young's modulus in the c direction is larger than that of the α phase. This could be attributed to the formation of additional Si-C bonds in the c direction of β.

IV. CONCLUSIONS

An all-electron and full potential first-principles method has been used to calculate the heats of formation, electronic structure, and elastic properties of the two polymorphs of Ti_3SiC_2.

(1) It was found that the energy of the β phase is higher than α, in agreement with the observation that β is a metastable phase;

(2) The topology analysis showed that Ti-Si bonding effect is significantly weaker in β than in α, giving less stabilizing effect for β. Si-C bonds, which are absent in α, are formed in β to provide additional stabilizing effect for β. In contrast to conventional thinking, there is no direction interaction between Ti atoms in both α and β;

(3) The DOS peak near the Fermi level of the α phase shifts to lower energy in the β phase, resulting in the decreased DOS at the Fermi level of β;

(4) The polycrystalline elastic constants and sound velocities deduced from calculated single crystal elastic constants were found to be consistent with the experimental results. The β phase is generally a little softer than the α phase;

(5) As revealed by the direction dependent Young's modulus, there is only limited elastic anisotropy in Ti_3SiC_2. For α, Young's modulus is minimum in the c direction and maximum in the directions 42° from c. For β, the maximum lies in the c direction, presumably because of the formation of Si-C bonds in this direction.

TABLE V: Calculated elastic constants (c_{ij} in GPa) and Cauchy ratio of the Ti_3SiC_2 polymorphs.

	c_{11}	c_{12}	c_{13}	c_{33}	c_{44}	c_{12}/c_{66}	c_{13}/c_{44}
α	360	84	101	350	158	0.61	0.64
β	360	86	89	348	120	0.63	0.74

TABLE VI: The bulk, shear, Young's moduli (B, G, E in GPa), Poisson's ratio (ν), density (ρ in g/cm^3), longitudinal, transverse, average elastic wave velocity (v_l, v_s, v_m in km/s), and the Debye temperature (θ_D in K) for polycrystalline Ti_3SiC_2 obtained from experiments or the calculated single crystal elastic constants.

		B	G	E	ν	ρ	v_l	v_s	v_m	θ_D
α	Experiment[52,a]	185	139	333	0.20	4.47	9.10	5.57	6.14	795[c]
	Experiment[52,b]	187	142	339	0.20	4.5	9.14	5.61	6.20	804[c]
	Experiment[51]	179	134	322	0.20	4.5	8.95	5.45	6.02	784[d]
	Experiment[54]	181								
	Experiment[53]	206								
	Calculation	182	142	338	0.191	4.47	9.12	5.64	6.22	805
β	Calculation	177	129	311	0.207	4.45	8.86	5.39	5.95	769

[a]Fine-grained samples; [b]Coarse-grained samples; [c]Corrected based on ρ and v_m; [d]Based on results reported in Ref. 51, but corrected in Ref. 52.

Acknowledgments

This work was partly supported by the Director, Office of Science, Office of Basic Energy Sciences, Materials Sciences Division of the U.S. Department of Energy under Contract No. DE-AC03-76SF0098.

[1] M. W. Barsoum, Prog. Solid State Chem. **28**, 201 (2000).
[2] T. Goto and T. Hirai, Mater. Res. Bull. **22**, 1195 (1987).
[3] C. Racault, F. Langlais, and R. Naslain, J. Mater. Sci. **29**, 3384 (1994).
[4] S. Arunajatesan and A. Carim, J. Am. Ceram. Soc. **78**, 667 (1995).
[5] J. F. Li, W. Pan, F. Sato, and R. Watanabe, Acta Mater. **49**, 937 (2001).
[6] R. Yu, Q. Zhan, L. L. He, Y. C. Zhou, and H. Q. Ye, Philo. Mag. Lett. **83**, 325 (2003).
[7] R. Yu, Q. Zhan, L. L. He, Y. C. Zhou, and H. Q. Ye, Acta Mater. **50**, 4127 (2002).
[8] N. I. Medvedeva, D. L. Novikov, A. L. Ivanovsky, M. V. Kuznetsov, and A. J. Freeman, Phys. Rev. B **58**, 16042 (1998).
[9] B. Holm, R. Ahuja, and B. Johansson, Appl. Phys. Lett. **79**, 1450 (2001).
[10] L. Farber, I. Levin, M.W. Barsourn, T. EI-Raghy, and T. Tzenov, J. Appl. Phys. **86**, 2540 (1999).
[11] R. Yu, Q. Zhan, L. L. He, Y. C. Zhou, and H. Q. Ye, J. Mater. Res. **17**, 948 (2002).
[12] R. Yu, Ph.D dissertation, Institute of Metal Research, Chinese Academy of Sciences, 2002.
[13] J. Y. Wang, Y. C. Zhou, Phys. Rev. B **69**, 144108 (2004).
[14] See, e.g., J. R. Chelikowsky and S. G. Louie, eds., Quantum Theory of Real Materials (Kluwer Academic, Amsterdam, 1996).
[15] R. Ahuja, O. Eriksson, J. M. Wills, and B. Johansson, Appl. Phys. Lett. **76**, 2226 (2000).
[16] Y. C. Zhou, Z. M. Sun, X. H. Wang and S. Q. Chen, J. Phys. Cond. Matt. **13**, 10001 (2001).
[17] R. F. W. Bader, *Atoms in Molecules: A Quantum Theory* (Oxford University Press, New York, 1990).
[18] R. F. W. Bader, Chem. Rev. **91**, 893 (1991).
[19] P. Popelier, *Atoms in Molecules: An Introduction* (Pearson Education Ltd, Essex, 2000).
[20] P. Blaha, K. Schwarz, G. K. H. Madsen, D. Kvasnicka and J. Luitz, *WIEN2k, An Augmented Plane Wave + Local Orbitals Program for Calculating Crystal Properties* (Karlheinz Schwarz, Techn. Universität Wien, Austria), 2001. ISBN 3-9501031-1-2.
[21] P. Blaha, K. Schwarz, P. Sorantin, S.B. Trickey, Comput. Phys. Commun. **59**, 399 (1990).
[22] D. J. Singh, *Planewaves, Pseudopotentials and the LAPW Method* (Kluwer Academic, Boston, 1994).
[23] P. Hohenberg and W. Kohn, Phys. Rev. **136**, B864 (1964).
[24] W. Kohn and L. J. Sham, Phys. Rev. **140**, A1133 (1965).
[25] E. Sjöstedt, L. Nordström, and D. J. Singh, Solid State Commun. **114**, 15 (2000).
[26] G. K. H. Madsen, P. Blaha, K. Schwarz, E. Sjöstedt, and L. Nordström, Phys. Rev. B **64**, 195134, 2001.
[27] J. P. Perdew, K. Burke, and M. Ernzerhof, Phys. Rev. Lett. **77**, 3865 (1996).
[28] P. Blöchl, O. Jepsen, and O. K. Andersen, Phys. Rev. B **49**, 16223 (1994).
[29] W. Jeitschko and H. Nowotny, Monatsh. Chem. **98**, 329 (1967).

[30] E. Eberhart, M. M Donovan, and R. A. Outlaw, Phys. Rev. B **46**, 12 744 (1992).
[31] P. F. Zou and R. F. W. Bader, Acta Crystallogr. A **50**, 714 (1994).
[32] V. G. Tsirelson, P. F. Zou, T. Tang, and R. F. W. Bader, Acta Crystallogr. A **51**, 143 (1995).
[33] A. M. Pendás, A. Costales, and V. Luaña, Phys. Rev. B **55**, 4275 (1997).
[34] J. D. Fuhr, J. O. Sofo, A Saúl, Surf. Sci. **506**, 161(2002).
[35] N. Kioussis, M. Herbranson, E. Collins and M. E. Eberhart, Phys. Rev. Lett. **88**, 125501 (2002).
[36] J. F. Nye, *Physical Properties of Crystals* (Oxford University Press, Oxford, 1985).
[37] D. C. Wallace, *Thermodynamics of Crystals* (Wiley, New York, 1972).
[38] F. Jona and P. M. Marcus, Phys. Rev. B **66**, 094104 (2002).
[39] L. Fast, J. M. Wills, B. Johansson, and O. Eriksson, Phys. Rev. B **51**, 17 431 (1995).
[40] W. Voigt, Lehrbuch der Kristallphysik (Taubner, Leipzig, 1928).
[41] A. Reuss, Z. Angew. Math. Mech. **9**, 55 (1929).
[42] R. Hill, Proc. Phys. Soc. London **65**, 350 (1952).
[43] O. L. Anderson, J. Phys. Chem. Solids **24**, 909 (1963).
[44] M. W. Barsoum, T. El-Raghy, C. J. Rawn, W. D. Porter, H. Wang, E. A. Payzant, and C. R. Hubbard, J. Phys. Chem. Solids **60**, 429 (1999).
[45] J. M. Cowley, *Diffraction Physics* (North-Holland Publishing Company, Amsterdam, 1981).
[46] J. W. Christian, *The Theory of Transformations in Metals and Alloys* (Pergamon Press, Oxford, 1975).
[47] R. Yu, unpublished.
[48] N. W. Ashcroft and N. D. Mermin, *Solid State Physics* (Saunders College Publishing, Philadelphia, 1976).
[49] J. K. Burdett, *Chemical Bonding in Solids* (Oxford University Press, Oxford, 1995).
[50] P. Finkel, M. W. Barsoum, and T. El-Raghy, J. Appl. Phys. **85**, 7123 (1999).
[51] P. Finkel, M. W. Barsoum, and T. El-Raghy, J. Appl. Phys. **87**, 1701 (2000).
[52] A. Onodera, H. Hirano, T. Yuasa, N. F. Gao, and Y. Miyamoto, Appl. Phys. Lett. **74**, 3782 (1999).
[53] M. W. Barsoum, private communication.

FIGURE CAPTIONS:

FIG. 1. Structure models of Ti_3SiC_2. α and β refer to the two polymorphs, respectively. α and β phases have the same space group ($P6_3/mmc$). The carbon atoms located in the octahedral interstices between Ti layers are represented by the smallest balls, one of which is indicated by an arrow.

FIG. 2. Calculated total valence charge densities (electron/Å ^{3}) for the $(11\bar{2}0)$ plane of (a) α, and (b) β.

FIG. 3. Difference charge densities (electron/Å^3) of (a) α, and (b) β. Dotted and solid lines denote negative and positive values in difference densities respectively.

FIG. 4. Band structures of (a) α, and (b) β.

FIG. 5. Band structure of the β phase in character plotting mode, showing (a) Si p_z, (b) Ti2 (d_{xz}+d_{yz}), (c) C p_z, and (d) Ti2 ($d_{x^2-y^2}$+d_{xy}) character bands.

FIG. 6. The total and partial DOS curves of (a) α, and (b) β.

FIG. 7. Schematic of the Bloch function of Si s orbitals at K point ($2\pi/3$, $2\pi/3$, 0) in the Brillouin zone of Ti_3SiC_2.

FIG. 8. Direction dependent Young's modulus of (a) α, and (b) β.

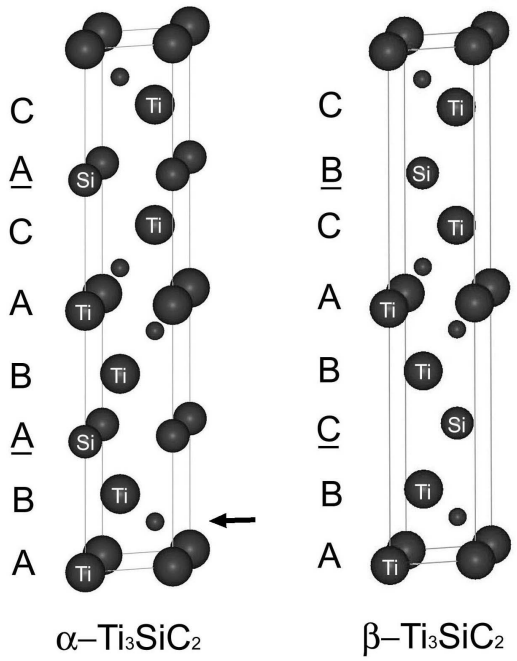

FIG. 1. Structure models of Ti_3SiC_2. α and β refer to the two polymorphs, respectively. α and β phases have the same space group ($P6_3/mmc$). The carbon atoms located in the octahedral interstices between Ti layers are represented by the smallest balls, one of which is indicated by an arrow.

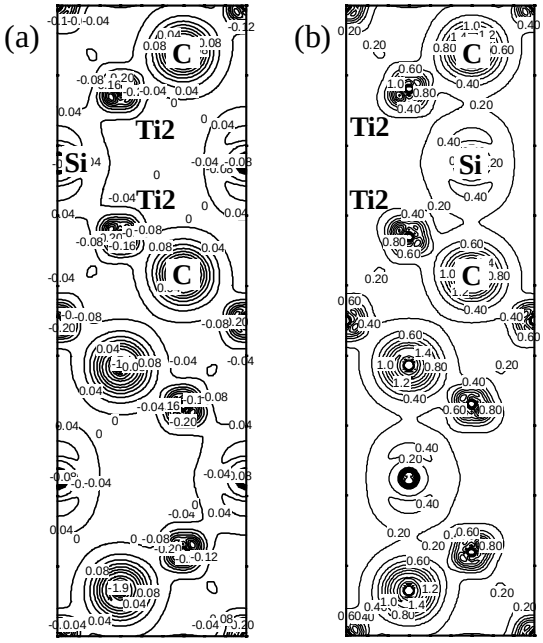

FIG. 2. Calculated total valence charge densities (electron/Å^3) for the $(11\bar{2}0)$ plane of (a) α, and (b) β.

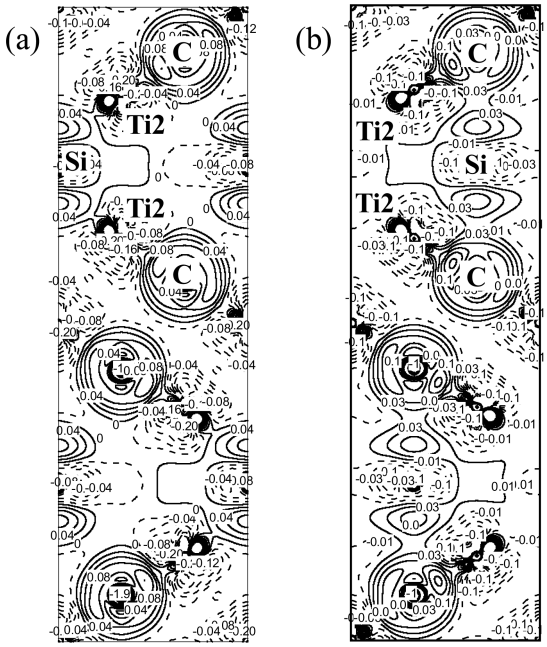

FIG. 3. Difference charge densities (electron/Å^3) of (a) α, and (b) β. Dotted and solid lines denote negative and positive values in difference densities respectively.

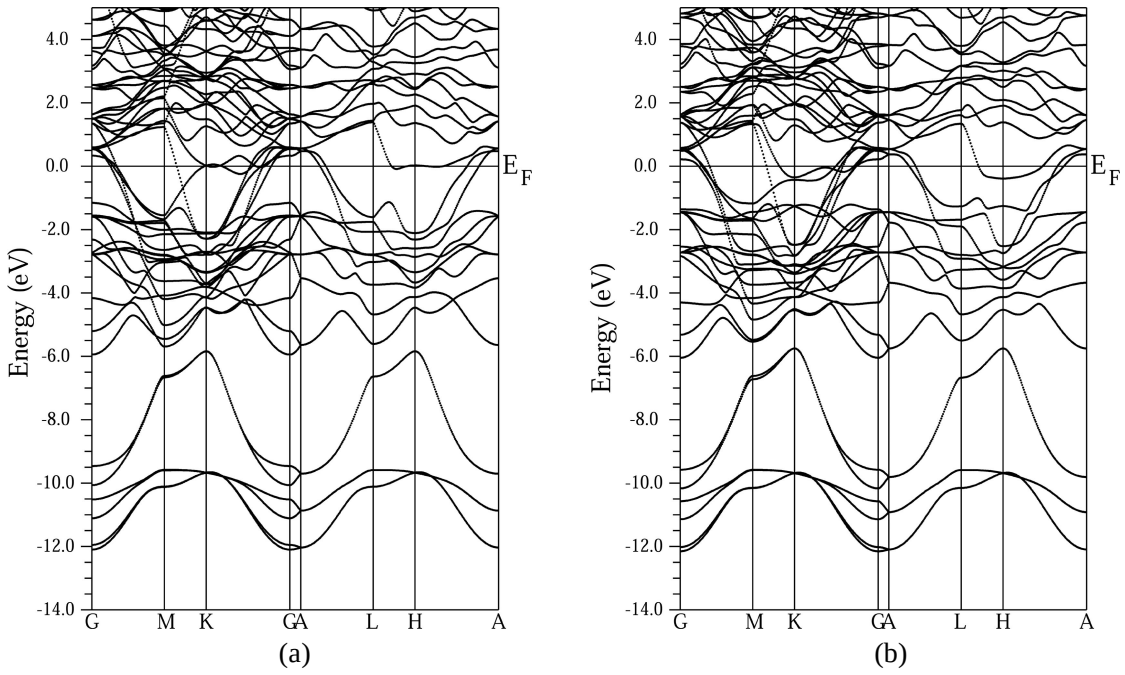

FIG. 4. Band structures of (a) α, and (b) β.

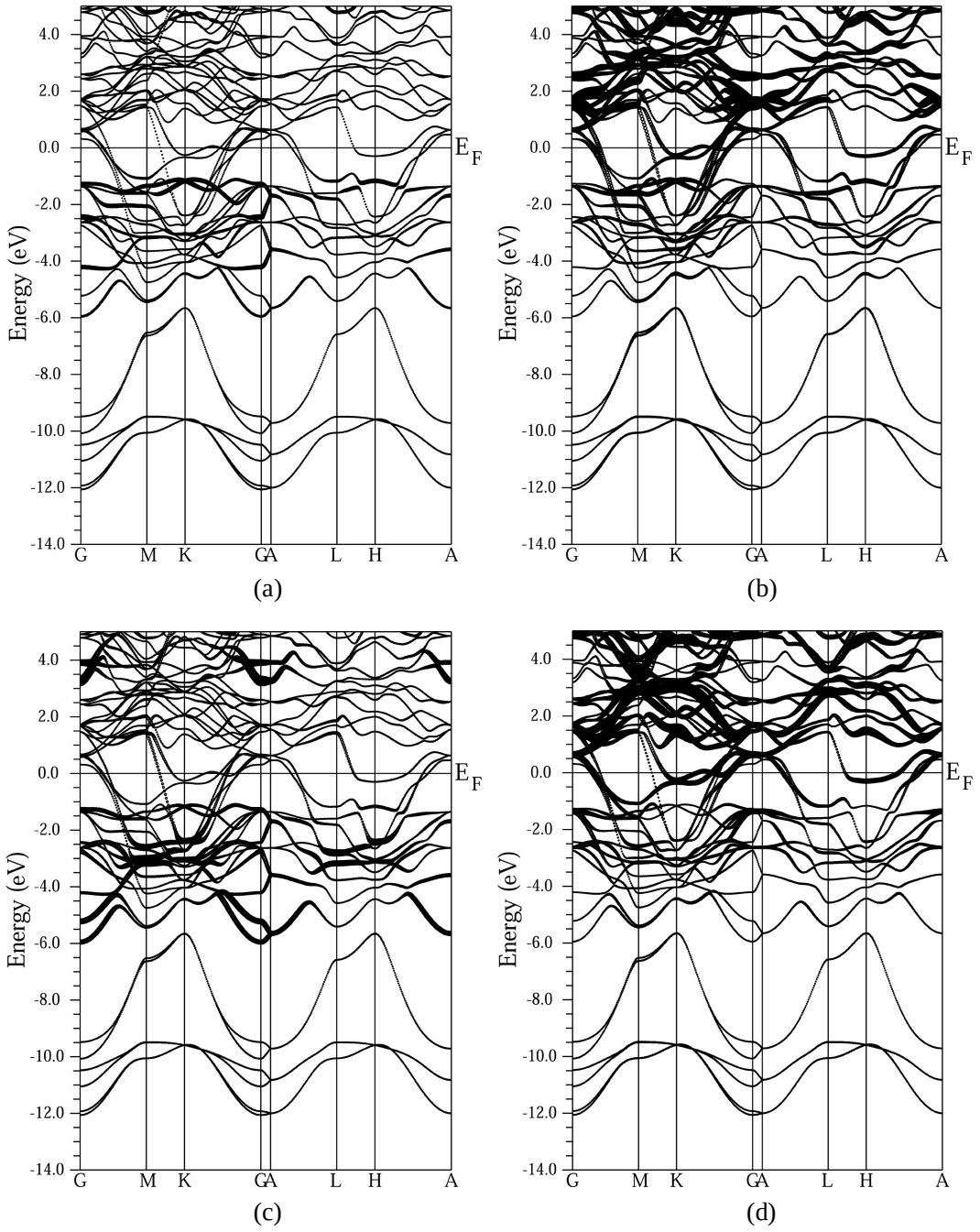

FIG. 5. Band structure of the β phase in character plotting mode, showing (a) Si p_z, (b) Ti2 (d_{xz}+d_{yz}), (c) C p_z, and (d) Ti2 (d_{x2-y2}+d_{xy}) character bands.

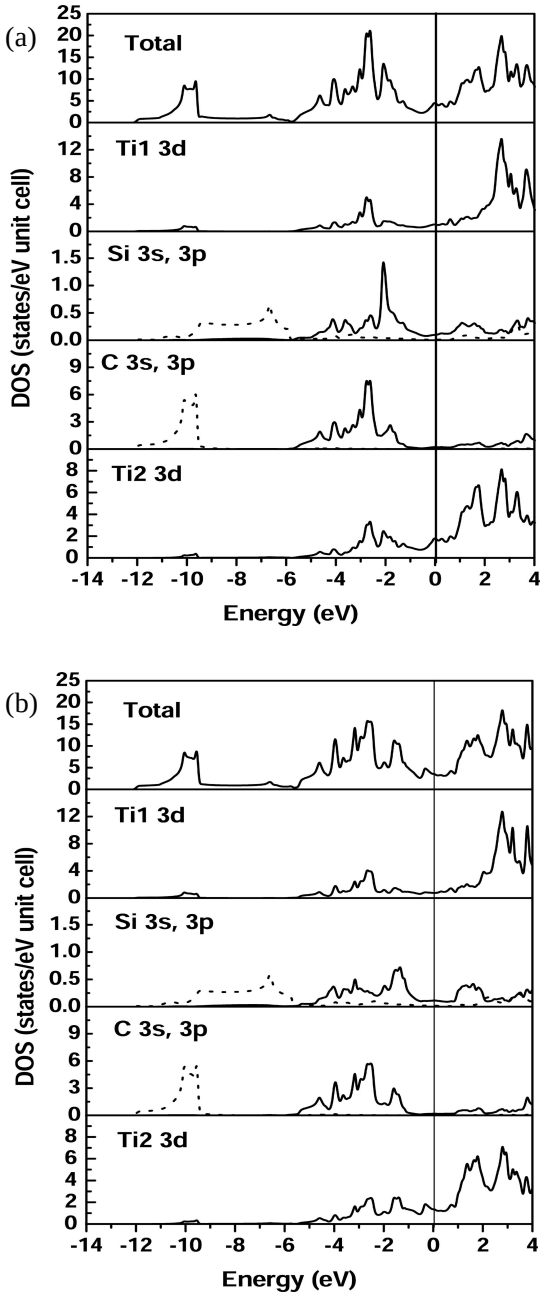

FIG. 6. The total and partial DOS curves of (a) α, and (b) β.

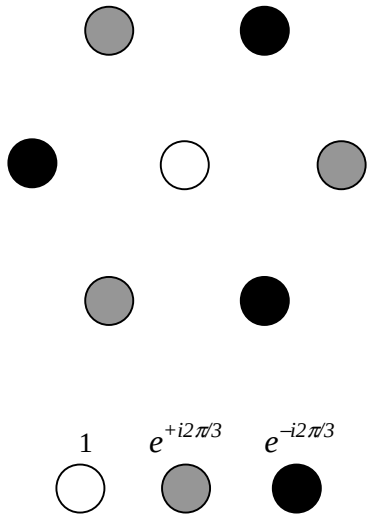

FIG. 7. Schematic of the Bloch function of Si *s* orbitals at K point ($2\pi/3$, $2\pi/3$, 0) in the Brillouin zone of Ti_3SiC_2.

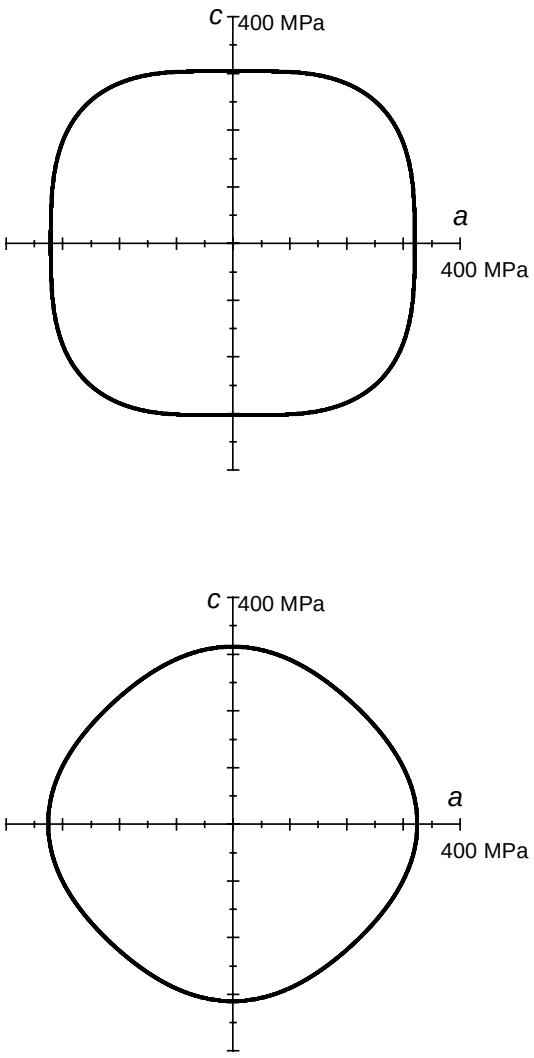

FIG. 8. Direction dependent Young's modulus of (a) α, and (b) β.